

# The chamfered bend two, four and eight-way SIW power dividers analysis for millimeter wave applications using the quick finite element method

Benzerga Fellah<sup>1</sup>, Nabil Cherif<sup>2</sup>, Mehadji Abri<sup>3</sup> and Hadjira Badaoui<sup>3</sup>

<sup>1</sup>Electrotechnical Department, Mascara University, Algeria.

<sup>2</sup>LSTE, Mascara University, Algeria.

<sup>3</sup>Department of Telecommunications, Abou Bekr Belkaid University, Tlemcen 13000, Algeria.

Corresponding author: (e-mail: [nabil.cherif@univ-mascara.dz](mailto:nabil.cherif@univ-mascara.dz))

**ABSTRACT** In this paper, we propose three kinds of substrate-integrated waveguide (SIWs) based chamfered bend power divider junctions provide equal power distribution to all output ports while maintaining high isolation and operating in the 54 GHz to 60 GHz frequency band. The advantages of the SIW technology are ease of design, fabrication and low form and full integration with planar printed circuits. In this case, the concept of the SIW H-plane power divider is implemented using a rigorous two-dimensional quick finite element method (2D-QFEM) programmed by MATLAB software. The numerical performance of this method is the Quick simulation time for using the mesh with Delaunay regularization in two dimensions, if we increase the mesh the FEM gives better results. This paper presents the transmission coefficient, return loss and the electric field distribution. The results obtained from QFEM were compared with those provided by HFSS for validation. When using the discretization with the Delaunay procedure only in two dimensions, we notice that the calculated simulation time decreases with good precision.

**INDEX TERMS** Millimeter Wave band, Chamfered bend Quick finite element method (2D-QFEM), Substrate integrated waveguide (SIW), Delaunay procedure

## I. INTRODUCTION

In addition to the broad class of microwave and millimeter-waveguide components as evidenced by the researches [1], we find that SIW technologies (bends and power dividers) are of particular interest, which is why they have numerous advantages in millimeter applications [2, 3]. The design of high-performance microwave components requires specific and accurate characterization of each component as antennas, couplers, filters, and diplexers [4-6]. High performance, low cost and small size are all requirements for these components. However, analyzing a 3D structure, which is not easy integrated with planar circuits (PCs), is very expensive for complex circuits. In fact, the advantages of this new technology are developed for precise simulation of these components. To analyze these types of waveguides, rigorous numerical methods are required, which are presented in [7-8]. Currently, the quick finite element method (QFEM) plays an important role in the analysis of various problems related

to electromagnetics, whether in simple structures such as waveguides in antenna complex [9], mixers and oscillators [10, 11]. The QFEM method is one of the CAD tools for microwave component analysis due to its speed and accuracy. The main advantage of these methods is the use of unstructured meshes, which increases the ability to accurately discretize complex geometries. In these cases, numerical techniques like QFEM are more flexible and easier to adapt to changes in discontinuous structure. The finite element method programmed in the MATLAB® environment is used for the analysis and design of SIW power divider. Finite element formulations are not easy to program because they allow lengthy and complex analytical formulations to be developed before application.

In the [15], we proposed SIW component curvatures in the 58-63 GHz range for 90° SIW curvature and circular SIW curvature in the 57-68 GHz range, as well as 1 × 4 and Eight-way\_SIW power distributions a 2D-FEM was proposed and analyzed in the range of 50 to 75 GHz. The obtained results

are compared with the CST simulation results. In this paper, we analyze and optimize two way, four-way and eight-way tilted SIW power dividers operating in the range of 54 to 60 GHz. These junctions operating in the millimeter waveband are proposed and analyzed using the two-dimensional quick finite element method (2D-QFEM), the results are compared with those of the Ansoft HFSS simulator. The work of this paper is organized as follow: first, we designed an architectural SIW power divider with chamfered bends and presented the results. Then we will discuss the (Two-way, four-way and eight-way) power dividers with several topologies in the architecture. We compared the simulation results of the 2D finite element method with the simulation results of the Ansoft HFSS software.

## II. 2D-QFEM IMPLEMENTATION

We exited the dominant fundamental TE<sub>10</sub> mode for the waveguide feeding. The FEM is used in the area  $\Omega$ , which is completely encircled by a perfectly conducting wall.  $\Gamma_0, \Gamma_1 \dots \Gamma_i, (i = 1 \dots n)$  is the contours of the ports as shown in Figure. 1. Our analyzed based on the present procedure [13]. The set of mode TE<sub>10</sub> that must be used to represent the components of the electric  $E_y$  and magnetic  $H_x$  field into each waveguide section, when the ports  $j$  are present.

The electric field scattered by the discontinuity in the inhomogeneous junction can be represented by an analytically known function satisfying the Helmholtz scalar equation. [12, 13].

$$\nabla_t \left( \frac{1}{\mu_r} \nabla_t E_y \right) + K_0^2 \varepsilon_r E_y = 0 \quad (1)$$

The above boundary conditions are:

$$E_y = 0, k = 1, 2, 3 \dots \quad (2)$$

On the waveguide wall  $\Gamma_0$ :

$$E_{y/\Gamma_k} = E_{ywg}^k, k = 1, 2, 3 \dots \quad (3)$$

$$H_{x/\Gamma_k} = H_{xwg}^k, k = 1, 2, 3 \dots \quad (4)$$

$$\frac{\partial E_y}{\partial z} \Big|_{\Gamma_k} = \frac{\partial E_{ywg}^k}{\partial z}, k = 1, 2, 3 \dots \quad (5)$$

$K$  is an integer

$\varepsilon_r$  is the relative dielectric permittivity.

$K_0$  is the propagation constant in the air

Let's utilize weighting functions that are arbitrarily differentiable, and using the weighted residual method, we can

replace equations (1), (2), (3), and (5) with:

$$\iint_{\Omega} W \nabla_t \left( \frac{1}{\mu_r} \nabla_t E_y \right) d\Omega + \iint_{\Omega} k_0^2 \varepsilon_r W E_y d\Omega = 0 \quad (6)$$

$$\int_{\Gamma_0} \overline{W} E_y d\Gamma_0 = 0 \quad (7)$$

$$\int_{\Gamma_k} \overline{W} E_y d\Gamma_k = \int_{\Gamma_k} \overline{W} E_{ywg}^k d\Gamma_k, k = 1, 2, 3 \dots \quad (8)$$

$$\int_{\Gamma_k} \overline{W} \frac{\partial E_y}{\partial z} d\Gamma_k = \int_{\Gamma_k} \overline{W} \frac{\partial E_{ywg}^k}{\partial z} d\Gamma_k, k = 1, 2, 3 \dots \quad (9)$$

$\mu_r$  is the substrate dielectric's relative permeability.

We derive the weak form of the Helmholtz equation by using Green's identity to (6) and using equation (9).

$$\iint_{\Omega} W \nabla_t \left( \frac{1}{\mu_r} \nabla_t E_y \right) d\Omega - k_0^2 \iint_{\Omega} \varepsilon_r W E_y d\Omega - \int_{\Gamma_k} W \frac{\partial E_{ywg}^k}{\partial z} d\Gamma_k = 0, k = 1, 2, 3 \dots \quad (10)$$

The solution for each element (e) is required under an approximate function  $\overline{E}_y^{(e)}$  of the form:

$$\overline{E}_y^{(e)}(x, y) = \sum_{j=1}^{N^{(e)}} \overline{E}_{y_j}^{(e)} \alpha_j^{(e)}(x, y) \quad (11)$$

$\overline{E}_{y_j}^{(e)}$  and  $\alpha_j^{(e)}(x, y), (j = 1, 2, \dots, N^{(e)})$  are the coefficients and the set of nodal-shape functions, respectively.  $W_i^{(e)}$  is the weight function equal to the shape functions,  $W_i^{(e)} = \alpha_i^{(e)}(x, y), (i = 1, 2, \dots, N^{(e)})$ .  $R_i^{(e)}$  is the residual with respect to the  $i^{\text{th}}$  weighting function, with:

$$\frac{1}{\mu_r} \iint_{\Delta^{(e)}} \nabla_t \alpha_j^{(e)} \nabla_t \overline{E}_y^{(e)} d\Omega - k_0^2 \varepsilon_r \iint_{\Omega} \alpha_j^{(e)} \overline{E}_y^{(e)} d\Omega \quad (12)$$

$$- \sum_{k=1}^N \int_{\Gamma_k^{(e)}} \alpha_j^{(e)} \frac{\partial E_{ywg}^k}{\partial z} d\Gamma_k = 0$$

The equation (12) can be written in matrix form:

$$\frac{1}{\mu_r} [S^{(e)}][\bar{E}_y^{(e)}] - k_0^2 \epsilon_r [T^{(e)}][\bar{E}_y^{(e)}] + \sum_{k=1}^N \{ [C_k^{(e)}][B_k] - [H_k^{(e)}] \} = [R^{(e)}] \quad (13)$$

Where:

$[S^{(e)}]$  and  $[T^{(e)}]$  present the usual local matrices of scalar nodal element.

$[\bar{E}_y^{(e)}]$  presents the vector of nodal unknown coefficients of element (e).

$[B_k]$  denotes a column vector, whose  $j^{\text{th}}$  input is the amplitude of the transmitted mode  $j$  at the port  $k$ . The contour integrals at the  $k = 1 \dots N$  ports provide  $[C_k^{(e)}]$  and  $[H_k^{(e)}]$

$[C_k^{(e)}]$  and  $[H_k^{(e)}]$  are given by:

$$C_{k_m}^{(e)} = j\beta_m^{(k)} \int_{\Gamma_k^{(e)}} \alpha_j^{(e)} e_m^{(e)} d\Gamma_k^{(e)} \quad (14)$$

$$C_{k_m}^{(e)} = j\beta_m^{(k)} \frac{2}{\sqrt{a^{(k)}b}} \sqrt{k_0 Z_0} \quad (15)$$

$$\times \int_{\Gamma_k^{(e)}} \alpha_j^{(e)} \sin\left(\frac{m\pi}{a^{(k)}} X^{(k)}\right) d\Gamma_k^{(e)}$$

$$H_{k_i}^{(e)} = j\beta_1^{(l)} \delta_{k1} \int_{\Gamma_k^{(e)}} \alpha_j^{(e)} e_1^{(l)} d\Gamma_k^{(e)} \quad (16)$$

$$H_{k_i}^{(e)} = j\beta_1^{(l)} \delta_{k1} \frac{2}{\sqrt{a^{(l)}b}} \sqrt{\frac{k_0 Z_0}{\beta_1^{(l)}}} \quad (17)$$

$$\times \int_{\Gamma_k^{(e)}} \alpha_j^{(e)} \sin\left(\frac{\pi}{a^{(l)}} X^{(l)}\right) d\Gamma_k^{(e)}$$

$\beta_m^{(k)}$  denotes the phase constant in the waveguide.

$\delta_{k1}$  is the Kronecker's delta.

### III. ARCHITECTURE AND RESULTS

This section describes other power divider topologies based on SIW technology. We will deal chamfered bend structures, these junctions are designed on a low loss Arlon Cu 217 LX substrate with dielectric constant  $\epsilon_r = 2.2$  and  $\tan\delta = 0.0009$ . The substrate thickness is 0.508 mm. Note that a Two-way power divider operates for cut-off frequency of 43 GHz. Therefore, the structure of Ansoft HFSS is optimized. These conversions operate in the V-band between 54 GHz and 60 GHz. In figure.1, we outline the topology of the Two-

waypower divider and its network, with is generated the mesh by the finite element method according to the Delaunay procedure [14]. Of course, the structure is surrounded by walls type PEC (Perfect Electric Conductor) and this to limit the discretization and optimize the computing time.

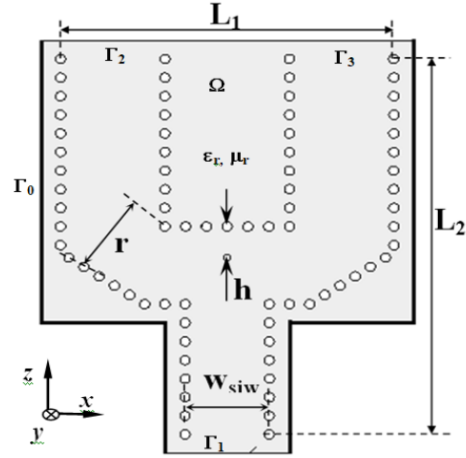


FIGURE 1. The Two-way SIW power divider structure in the H plane.

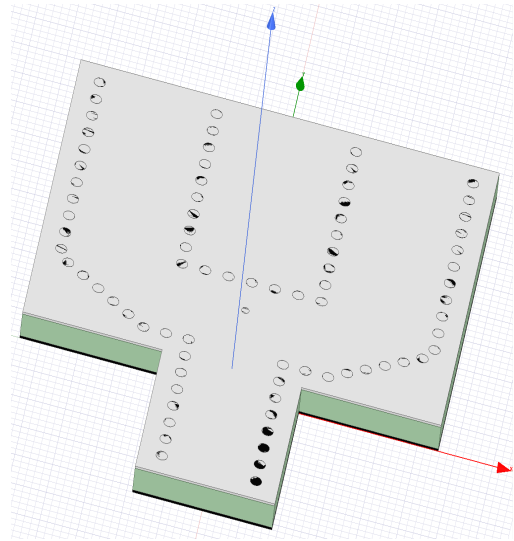


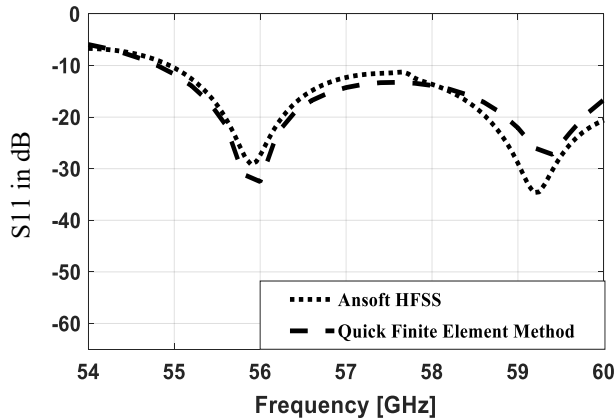
FIGURE 2. The Two-way SIW power divider structure in 3D.

Figure 2 represents the optimized two-way SIW power divider in 3D form.

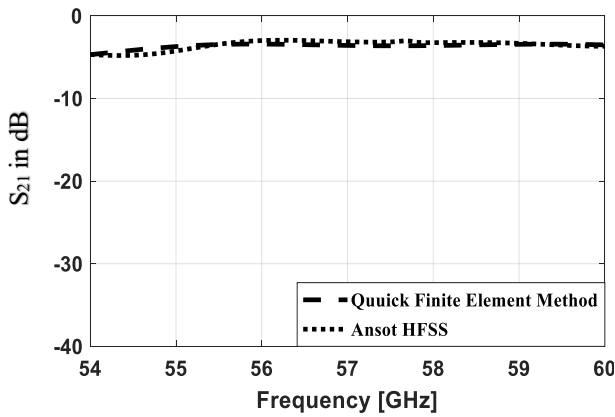
TABLE I. Parameters of the waveguide power divider.

Geometry name	Geometry	Sizes (mm)
The SIW guide width	W <sub>siw</sub>	2.51
Via Diameter	d	0.3
Via space	S	0.6
Via hole space	h	1
Diameter of the bend	r	1.75
Length	L <sub>1</sub>	7.8
Width	L <sub>2</sub>	12.71
Via hole diameter	d <sub>h</sub>	0.3
Wall distance	d <sub>1</sub> , d <sub>2</sub>	0.75

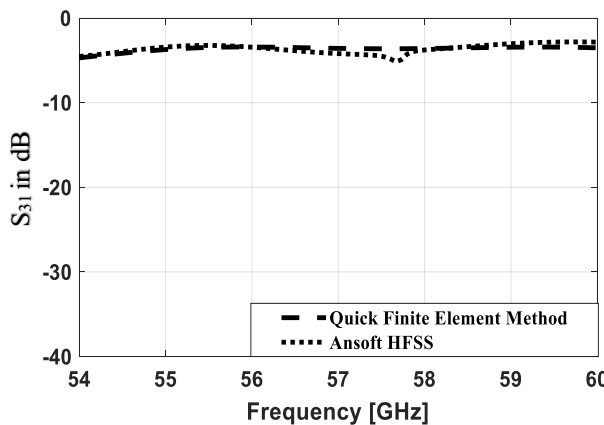
To analyze the performance of the SIW power divider shown in Fig. 1, the reflection and transmission coefficients of the  $1 \times 2$  SIW power divider with chamfered bend are obtained by a two-dimensional quick finite element 2D-QFEM. The method and Ansoft HFSS simulation results are shown in Figure 3, respectively. (a), (b) and (c) in the frequency range between 54 and 60 GHz.



(a)



(b)



(c)

**FIGURE 3.** Results for  $1 \times 2$  power divider with chamfered bend, (a) Reflection coefficients S11, (b) (c) Transmission coefficients S12 and S13.

According to the simulation comparison results provided in Figure 3. Reflection coefficients and transmission we see good consistency is obtained between the two results of QFEM and Ansoft HFSS. It should be noted that two peaks provided by QFEM at 55.9 GHz and 59.2 GHz were given by HFSS. Both graphs show that the transmission is only possible from 54 GHz; this is clear in Figures 3. (b) and (c).

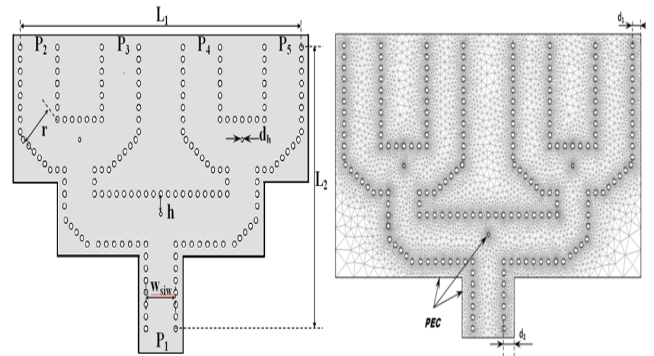


**FIGURE 4.** The Four-way SIW power divider structure with chamfered bend and center via ( $L_1 = 62.4$  mm,  $L_2 = 38.69$  mm), (a) H-plane top view, (b) Mesh according to the Delaunay procedure.

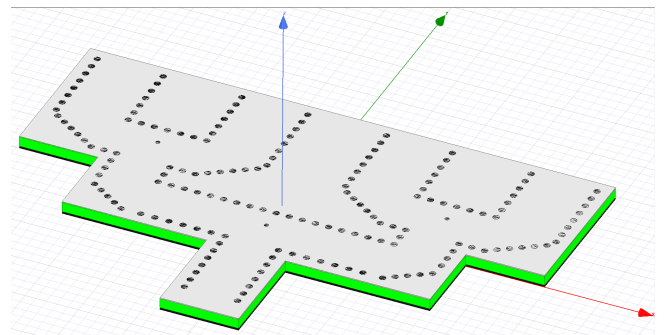
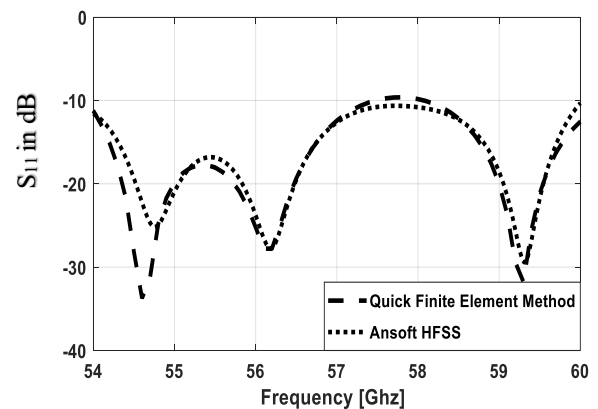
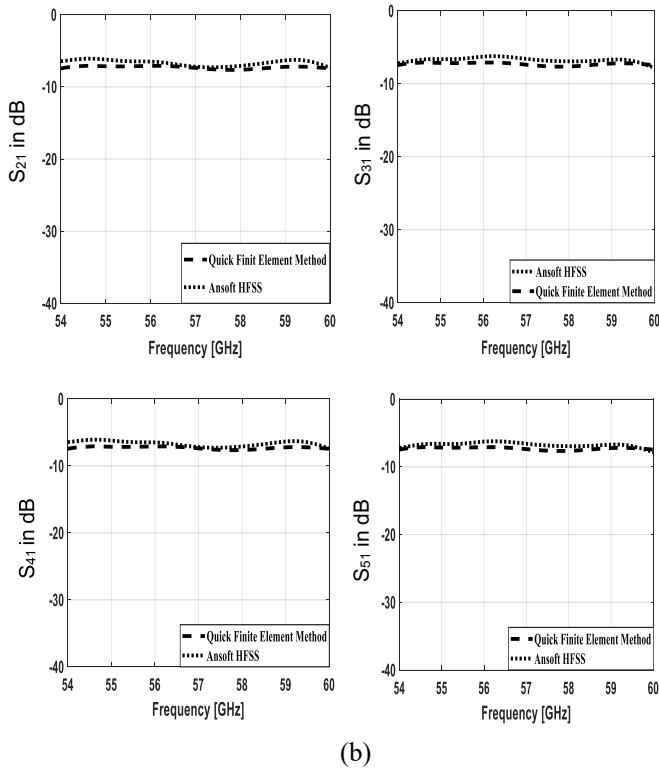


**FIGURE 5.** The Four-way SIW power divider structure in 3D

Figure 5 represents the optimized four-way SIW power divider in 3D form.



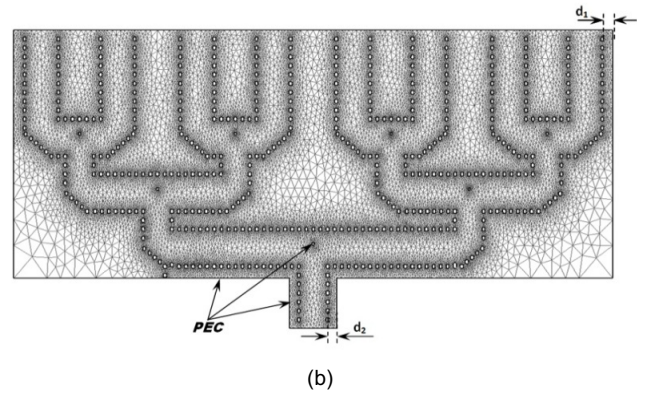
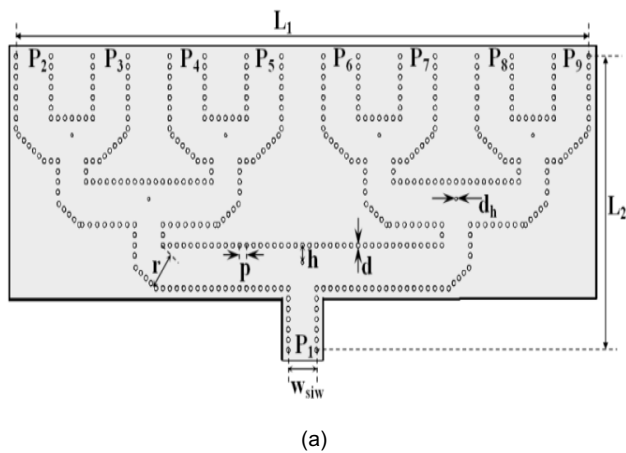
(a)



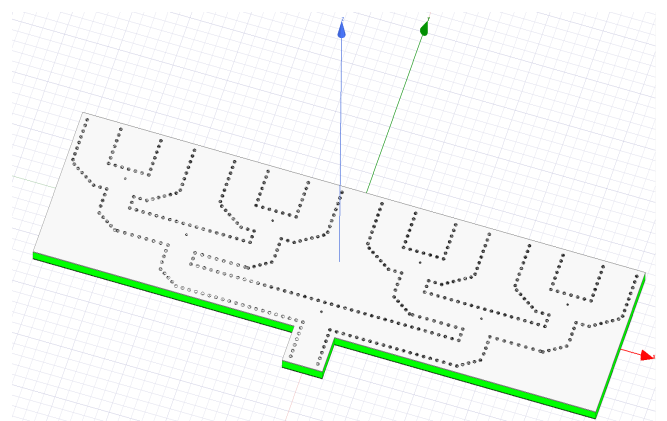
**FIGURE 6.** Comparison of finite element method simulation results and HFSS for 1x4 power divider. (a) Reflection coefficients S11, (b) Transmission coefficients S12, S13, S14 and S15.

Figure 6 present, reflection coefficients and transmission we see two peaks provided by QFEM at 56.2 GHz and 59.3 GHz were given by HFSS.

Performance of the quick finite elements method (QFEM), It is useful to illustrate in fig. 5 (b) the mesh of the structure of the Eight-way power divider subdivided in to tetrahedral triangular cells generated by the Matlab simulator according to the Delaunay procedure.

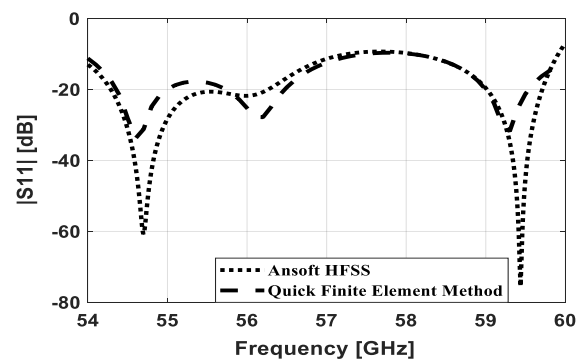


**FIGURE 7.** The Eight-way power divider structure in H-plane with chamfered bend and hole via center, (a) the parameters are defined in table.1 and  $L1 = 100.51$  mm and  $L2 = 49.95$  mm, (b) the Delaunay refinement mesh of the power divider.



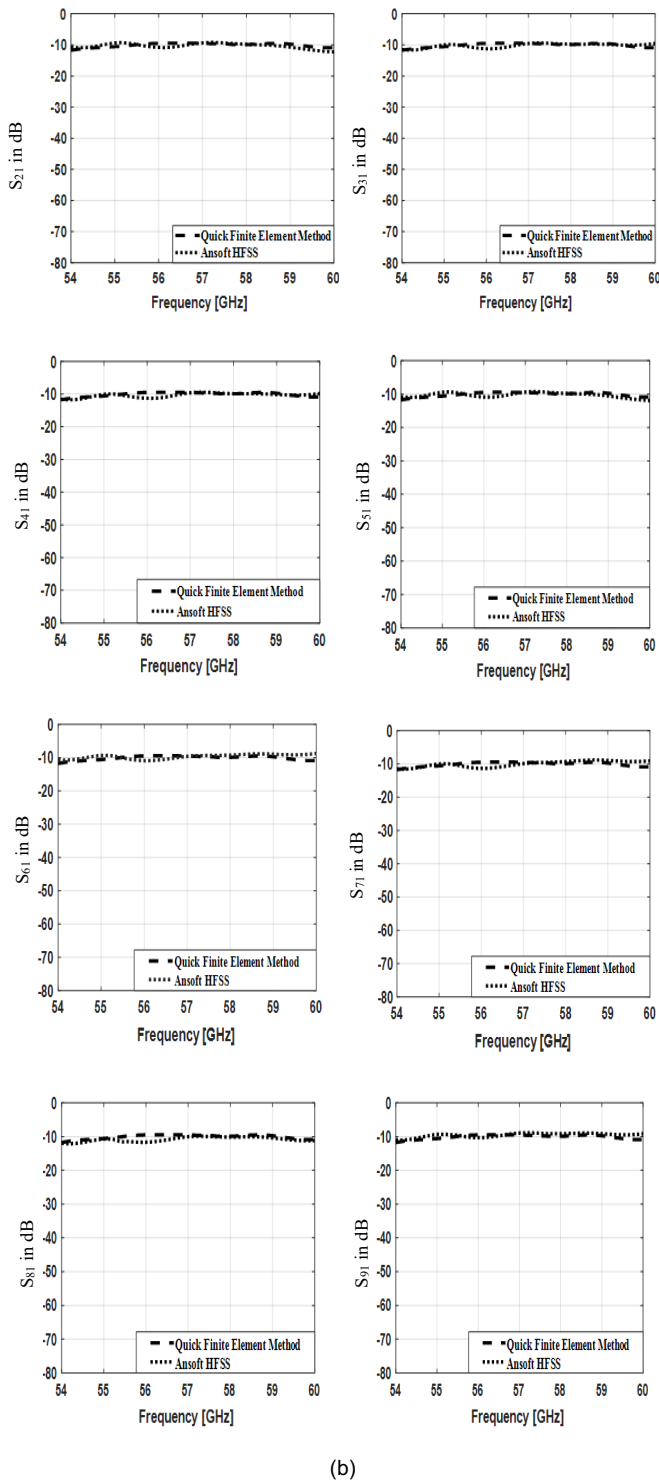
**FIGURE 8.** The 1x 8 power divider structure in 3D

Figure 8 represents the optimized two-way SIW power divider in 3D form. The comparison of the reflection and transmission coefficient results of the V-band of the power divider shown in Figure 7 in the frequency range of 54-60 GHz by the quick finite element method and Ansoft HFSS software is shown in Figure 9 respectively.



(a)





**FIGURE 9.** Results of the Eight-way SIW power divider obtained between QFEM and HFSS, (a) Reflection coefficients  $S_{11}$  and (b) Transmission coefficients  $S_{11}$ .

In Figure 10, we plot the  $E_y$  field distribution of the  $TE_{10}$  fundamental mode within the waveguide junction obtained by the QFEM method. It can be seen that the dielectric vias play an important role in concentrating the field splitting, thereby reducing reflections due to discontinuities.

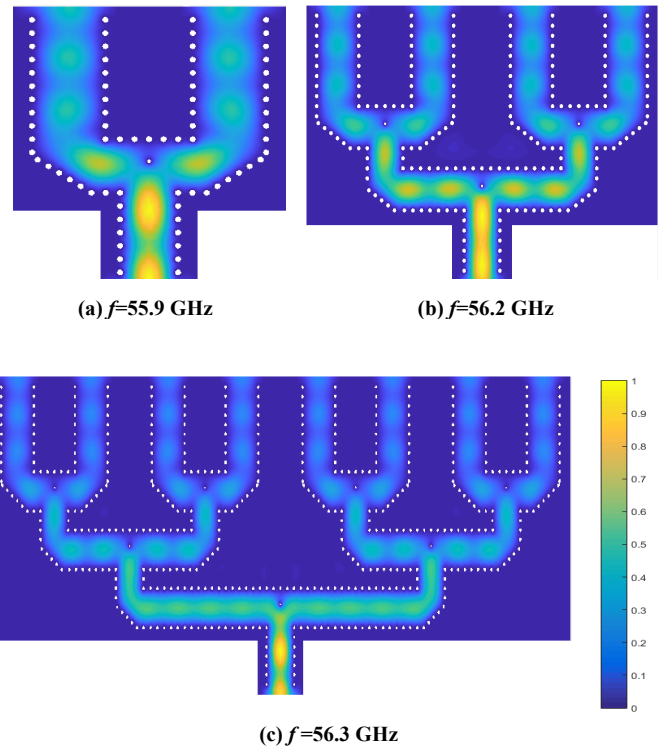


**FIGURE 10.** Electric-fields distribution within the SIW power dividers obtained with the quick finite element method. The fields are simulated respectively of the SIW power divider: (a) The Two-way ports, (b) the 1x4 ports and (c) the 1x8 ports

#### IV. COMPARISON OF THE SIMULATION TIME

A comparison of the simulation time with the number of components generated by QFEM and Ansoft HFSS for the different proposed power divider structures is shown in Table 2.. The structures to be simulated in the computer with CPU running at 2.7 GHz , 8go memory and NVIDIA GeForce GT 330M GPU.

**TABLE 2.** Comparison of the simulation time with QFEM and Ansoft HFSS.

Number of elements (N)		Simulation Time(s)	
		2D-QFEM	Ansoft 3D-HFSS
Two-way power divider	N = 7971	2.20	93.7
1x4 power divider	N =21127	9.02	155.3
1x8 power divider	N =52094	38.72	291.1

In table.2, we observe that the increase in the number of elements is accompanied by a slight increase in simulation time of QFEM method and a faster increase in the case of Ansoft HFSS simulator. Note that, from the number of elements of different structures, the QFEM method presents a simulation time lower than the Ansoft HFSS, as well as a

slightly higher simulation time is shown by HFSS simulator, the number of elements is increased, this causes the simulation time to increase. For example in the second power divider structure, the number of elements is  $N = 21127$ , the simulation time with HFSS is greater 17 times than QFEM.

## V. CONCLUSION

This article is dedicated to the application of a 2D quick finite element method 2D-QFEM programmed in the MATLAB® environment to analyze V-band based SIW technology transitions in the frequency range from 54 to 60 GHz. The target component is the analysis and validation of a quick finite element method of a chamfered bend SIW power divider. We also explored different topologies for  $1 \times 2$ -port, Four-way-port, and Eight-way-port chamfer power dividers. The simulation results of the 2D-QFEM and the Ansoft HFSS simulator are compared to test the method used.

The consistency of the large number of findings demonstrates the validity of this approach and the possibility of analyzing and simulating transitions in SIW techniques using a two-dimensional finite element method. Future analyses will be devoted to designing SIW antennas and array antennas using power dividers.

## REFERENCES

- [1] M. Henry, C. Free, B. Izqueirdo, J. Batchelor, and P. Young, "Millimeter wave substrate integrated waveguide antennas: Design and fabrication analysis", *IEEE Trans. Adv. Packag.*, vol. 32, no. 1, pp. 93–100, 2009.
- [2] Fellah Benzerga and Abri Mehadjji, "Design of Millimeter Substrate Integrated Wave Guide MSIW analysis by the Quick Finite Element Method (QFEM)", *International Conference on Advanced Communication Systems and Signal Processing, ICOSIP*, 8-9 November Tlemcen, Algeria, 2015.
- [3] L. Yan, W. Hong, G. Hua, J. Chen, K. Wu, and T. J. Cui, "Simulation and experiment on SIW slot array antennas", *IEEE Microw. Wireless Compon. Lett.*, vol. 14, no. 9, pp. 446–448, 2004.
- [4] Robab Kazemi, Aly E. Fathy, and Ramezan Ali Sadeghzadeh, "Dielectric Rod Antenna Array With Substrate Integrated Waveguide Planar Feed Network for Wideband Applications", *IEEE transactions on antennas and propagation*, vol. 60, no. 3, pp. 1312–1219, 2012.
- [5] J. Tang, W. Hong, J.-X. Chen, G. Q. Luo and K. Wu, "Development of millimetre-wave planar diplexers based on complementary characters of dual-mode substrate integrated waveguide filters with circular and elliptic cavities", *IEEE Trans. Microwave TheoryTech.*, vol. 55, pp. 776–782, 2007.
- [6] J. X. Chen, W. Hong, Z. C. Hao, H. Li, and K. Wu, "Development of a low cost microwave mixer using a broadband substrate integrated waveguide (SIW) coupler", *IEEE Microw. Wireless Compon. Lett.*, vol. 16, no. 2, pp. 84–86, 2006.
- [7] Arnieri, E. and G. Amendola, "Method of moments analysis of slotted substrate integrated waveguide arrays", *IEEE Transactions on Antennas and Propagation*, vol. 59, no. 4, pp. 1148–1154, 2011.
- [8] H. Sato, K. Sawaya, N. Arai, Y. Wagatsuma, and K. Mizuno, "Broadband FDTD analysis of Fermi antenna with narrow width substrate", in *Proceedings of the IEEE AP-S International Symposium*, Columbus, U.S.A, 2003, pp. 261–264.
- [9] L. Yan, W. Hong, G. Hua, J. Chen, K. Wu, and T. J. Cui, "Simulation and experiment on SIW slot array antennas", *IEEE Microw. Wireless Compon. Lett.*, vol. 14, no. 9, pp. 446–448, 2004.
- [10] J.-X. Chen, W. Hong, Z.-C. Hao, H. Li, and K. Wu, "Development of a low cost microwave mixer using a broadband substrate integrated waveguide (SIW) coupler", *IEEE Microw. Wireless Compon. Lett.*, vol. 16, no. 2, pp. 84–86, 2006.
- [11] Y. Cassivi and K. Wu, "Low cost microwave oscillator using substrate integrated waveguide cavity", *IEEE Microw. Wireless Compon. Lett.*, vol. 13, No. 2, pp. 48–50, 2003.
- [12] Coccioli, R. Pelosi, R. and Selleri, S, "Optimization of Bends in Rectangular Waveguide by a Finite Element-Genetic Algorithm Procedure", *Microwave and Optical Technology Letters*, vol. 16, pp. 287–290, 1997.
- [13] G. Pelosi, R. Coccioli, S. Selleri, "Quick Finite Elements for Electromagnetic Waves", Second Edition, Boston: Artech House, 2009.
- [14] Shewchuk, J.R., "Delaunay refinement algorithms for triangular mesh generation", *Comput. Geom.* vol. 47, pp. 741–778, 2014.
- [15] B. Fellah, M. Abri and H. Badaoui "Optimized bends, corporate  $1 \times 4$  and  $1 \times 8$  SIW power dividers junctions analysis for V-Band applications using a rigorous finite element method," *Arabian Journal for Science and Engineering*, vol. 41, no. 9 pp. 3335–3343, sep 2016.